Research Square

Preprints are preliminary reports that have not undergone peer review.
They should not be considered conclusive, used to inform clinical practice,
or referenced by the media as validated information.

Numerical analysis of free convection in a ternary hybrid nanofluid within a porous enclosure under inclined magnetic field, radiation, and internal heat generation

P. D. Selvi
Sri Padmavathi Mahila Visva Vidyalyam
Annuri Shobha
Sri Padmavathi Mahila Visva Vidyalyam
K. Venkatadri
Mohan Babu University (Erstwhile Sree Vidyanikethan Engineering College)
K Sudarmozhi
Saveetha School of Engineering, SIMATS
J. O. Akanni
jide28@gmail.com

Saveetha School of Engineering, SIMATS

Research Article

Keywords: Ternary hybrid nanofluid, Magnetohydrodynamic (MHD), Square enclosure, heat transfer, Porous medium, Finite difference Method, Free convection

Posted Date: March 20th, 2026

DOI: https://doi.org/10.21203/rs.3.rs-9131455/v1

License: This work is licensed under a Creative Commons Attribution 4.0 International License. Read Full License

Additional Declarations: No competing interests reported.

Numerical analysis of free convection in a ternary hybrid nanofluid within a porous enclosure under inclined magnetic field, radiation, and internal heat generation

P. D. Selvi[1], Annuri Shobha[2], K. Venkatadri[3], K Sudarmozhi[4*] and J. O. Akanni[4,5*]

[1]Department of Applied Mathematics, Sri Padmavathi Mahila Visva Vidyalyam, Tirupati, AP, India. selvi.pd2014@gmail.com
[2]Department of Applied Mathematics, Sri Padmavathi Mahila Visva Vidyalyam, Tirupati, AP, India. shobhaannuri123@gmail.com
[3]Department of Mathematics, Mohan Babu University (Erstwhile Sree Vidyanikethan Engineering College), Tirupati, A.P. 517102, India.
venkatadri.venki@gmail.com
[4] Department of Mathematics, Saveetha School of Engineering, SIMATS, Chennai, Tamil Nadu, India. sudarmozhik1033.sse@saveetha.com*
[5]Department of Mathematical and Computing Sciences, KolaDaisi University, Ibadan, Oyo State, Nigeria. jide28@gmail.com*

Abstract

This research presents a numerical investigation of free convection of a ternary hybrid nanofluid in a permeable enclosure under the impact of an inclined magnetic field, thermal radiation, and internal heat generation. The ternary hybrid nanofluid consists of a base fluid with dispersed nanoparticles of aluminum oxide, copper (*Cu*), and multi-walled carbon nanotubes to increase thermal conductivity. The governing equations for mass, momentum, and energy are formulated in nondimensional form and solved via the Marker-And-Cell (MAC) method on a staggered grid with a finite difference discretization scheme. The effects of key dimensionless parameters including Rayleigh number (*Ra*), Hartmann number (*Ha*), radiation (*Rd*), Darcy number (*Da*), and heat generation/absorption parameter (*Q*) on heat transfer characteristics are analyzed. The results show that increasing *Ra* from 10^3 to 10^6 enhances convective heat transfer, leading to a 192% increase in the average Nusselt number (Nu_a), whereas decreasing *Da* from 0.1 to 0.0001 suppresses convection and results in a 53% drop in Nu_a. The application of an external magnetic field (*Ha*=50) reduces energy transfer efficiency by 41%, confirming the suppressive effect of Lorentz forces. Conversely, increasing *Rd* from 0 to 5 significantly enhances radiative energy transfer, leading to a 229% rise in Nu_a. Internal heat generation (*Q*=5) weakens convective motion, reducing Nu_a by 12%, while heat absorption enhances convection and increases heat transfer. These findings highlight the strong interplay between buoyancy, magnetic field suppression, porous medium resistance, radiative heat transfer, and internal heat generation, demonstrating that ternary hybrid nanofluids can be optimized for various thermal management applications, including nuclear reactor cooling, MHD power generation, industrial heat exchangers, and electronic cooling systems.

Keywords: Ternary hybrid nanofluid, Magnetohydrodynamic (MHD), Square enclosure, heat transfer, Porous medium, Finite difference Method, Free convection.

1. INTRODUCTION

Free convection heat transfer in porous enclosures has been widely studied due to its significance in thermal energy storage, electronic cooling, nuclear reactor safety, and magnetohydrodynamic (MHD) power generation. Enhancing heat transfer in such systems is a critical research area, with nanofluids emerging as a promising solution. Nanofluids, which are engineered suspensions of nanoparticles in base fluids, display superior thermal properties associated with conventional fluids, leading to improved heat transport efficiency [1], [2]. Recent advancements in hybrid nanofluids, which trust multiple types of nanoparticles, have further optimized thermal conductivity, stability, and energy transport [3], [4]. However, most studies have focused on binary hybrid nanofluids, while the possibility of ternary hybrid nanofluids in MHD permeable enclosures under the inspiration of radiation and internal heat generation remains largely unexplored [5], [6].

The impact of porous media on natural convection is substantial, as it introduces flow resistance that alters the convection-diffusion balance. Several studies have analyzed the effect of Darcy number (Da), demonstrating that decreasing permeability reduces convective motion, shifting the dominant heat transfer mode from convection to conduction [7], [8]. Additionally, the interaction of MHD effects with nanofluid convection in porous enclosures has been widely investigated, showing that the application of an external magnetic field dampens convective flow due to the Lorentz force, thereby decreasing the overall heat transfer rate [9], [10]. Furthermore, studies have shown that the orientation of the applied magnetic field plays an important role in altering flow structures and convective heat transport [11], [12]. Such effects are crucial in engineering applications, including MHD-based energy conversion, nuclear reactor cooling, and electromagnetic heat control systems.

Another important mechanism influencing heat transfer in nanofluid-filled enclosures is thermal radiation, particularly in high-temperature applications. Studies have shown that neglecting radiative heat transfer can lead to significant underestimation of thermal performance in enclosures with large temperature gradients [13], [14]. Increasing the thermal radiation enhances the contribution of radiative energy transport, altering temperature distributions and increasing heat transfer efficiency [15], [16]. Similarly, internal heat generation and absorption are essential

considerations, as heat generation weakens convective motion by reducing buoyancy forces, while heat absorption enhances convective instability, leading to higher Nusselt numbers [17], [18]. These phenomena are particularly relevant in requests such as solar thermal collectors, nuclear energy systems, and electronic cooling technologies.

Despite extensive research on hybrid nanofluid convection in enclosures, most prior studies have been limited to single-component or binary hybrid nanofluids, while the energy advantages of ternary hybrid nanofluids remain underexplored [19], [20]. Ternary hybrid nanofluids, which include 3 diverse types of nanoparticles, have been shown to provide enhanced energy transfer properties due to synergistic improvements in thermal conductivity, viscosity, and stability [21], [22]. However, limited studies have investigated ternary hybrid nanofluids in porous enclosures under the combined impact of MHD effects, radiation, and internal heat generation [23], [24]. Additionally, many previous numerical studies have employed simplified computational techniques [35-37], whereas advanced approaches such as the MAC method offer greater accuracy in solving incompressible flow problems and complex convection-dominated heat transfer [25], [26].

The current study aims to numerically examine the free convection of a ternary hybrid nanofluid in a permeable enclosure under the combined possessions of an inclined magnetic field, thermal radiation, and internal heat generation. The governing equations are formulated in nondimensional form and solved using the MAC method on a staggered grid, employing a finite difference discretization scheme. The ternary hybrid nanofluid consists of water (H_2O) as the base fluid, with Al_2O_3, copper (Cu), and MWCNTs as nanoparticles, selected for their high thermal conductivity, improved stability, and superior energy transfer performance. The effects of key dimensionless parameters with *Ra*, *Ha*, *Da*, *Rd*, and *Q* on flow structure, temperature distribution, and energy transfer characteristics are systematically analyzed.

This study provides a complete quantitative analysis of the impact of these parameters on the average and local Nusselt numbers, offering valuable insights into the design and optimization of advanced thermal management systems. The findings have direct applications in MHD power generation, industrial heat exchangers, nuclear reactor cooling, electronic thermal management, and solar energy technologies. The rest of this manuscript is structured as follows: Section 2 presents the mathematical formulation, including the governing equations and boundary

conditions. Section 3 describes the numerical methodology, with an emphasis on the MAC method implementation. Section 4 discusses the results and parametric analysis, highlighting key findings related to flow behavior and heat transfer performance. Finally, Section 5 offers the conclusions and references for future research.

2. MATHEMATICAL FORMULATION

The mathematical modeling of free convection in a permeable enclosure filled with ternary hybrid nanofluid is essential to accurately describe the underlying transport phenomena, including fluid flow, energy transfer, and the possessions of magnetic fields and radiation. The current study as shown in **Figure 1** involves the formulation of governing equations based on the principles of fluid dynamics and heat transfer, incorporating additional effects due to porous media, a motivated magnetic field, and internal energy generation or absorption. The ternary hybrid nanofluid, comprising water and nanoparticles of Al_2O_3, copper (*Cu*), and MWCNT, exhibits enhanced thermophysical properties, such as higher thermal conductivity and improved heat transfer capabilities. The Thermo-physical properties details are in **Table 2**, and filled with the Al_2O_3, copper (*Cu*), and MWCNT, ternary hybrid nano-fluid featured in **Table 1.** These properties are integrated into the governing equations by defining effective parameters, with thermal conductivity, dynamic viscosity, and heat capacity, as functions of the nanoparticle volume fractions. The permeable medium is modeled using the Brinkman approximation, which accounts for viscous effects, and the impact of the inclined magnetic field is incorporated through Lorentz force terms in the momentum equations. Additionally, thermal radiation effects are modeled using the Rosseland approximation, enabling the inclusion of radiative energy transfer in the energy equation. To account for internal energy generation, a source term is introduced in the energy equation [28-34].

Dimensional Form

$$\frac{\partial u}{\partial x}+\frac{\partial v}{\partial y}=0 \tag{1}$$

$$\frac{\partial u}{\partial t^*}+u\frac{\partial u}{\partial x}+v\frac{\partial u}{\partial y}=-\frac{1}{\rho_{hnf}}\frac{\partial p}{\partial x}+\nu_{hnf}\left[\frac{\partial^2 u}{\partial x^2}+\frac{\partial^2 u}{\partial y^2}\right]$$

$$-\frac{\nu_{hnf}}{K}u+\frac{\sigma_{hnf}B_0^2}{\rho_{hnf}}(v\ sin\ sin\ \delta\ \ cos\ cos\ \delta\ -u\ sin^2\ \delta) \tag{2}$$

$$\frac{\partial v}{\partial t^*} + u\frac{\partial v}{\partial x} + v\frac{\partial v}{\partial y} = -\frac{1}{\rho_{hnf}}\frac{\partial p}{\partial y} + \nu_{hnf}\left[\frac{\partial^2 v}{\partial x^2} + \frac{\partial^2 v}{\partial y^2}\right] - \frac{\nu_{hnf}}{K}v$$

$$+\frac{\sigma_{hnf}B_0^2}{\rho_{hnf}}(u\,sin\,sin\,\delta\;\;cos\,cos\,\delta\;\; - v\,cos^2\delta) + \frac{(\rho\beta)_{hnf}}{\rho_{hnf}}g(T - T_c) \qquad (3)$$

$$\frac{\partial T}{\partial t^*} + u\frac{\partial T}{\partial x} + v\frac{\partial T}{\partial y} = \frac{k_{hnf}}{(\rho C_p)_{hnf}}\left[\frac{\partial^2 T}{\partial x^2} + \frac{\partial^2 T}{\partial y^2}\right] - \frac{1}{(\rho C_p)_{hnf}}\left(\frac{\partial q_{rx}}{\partial x} + \frac{\partial q_{ry}}{\partial y}\right) + \frac{Q_0}{(\rho C_p)_{hnf}}(T - T_c) \qquad (4)$$

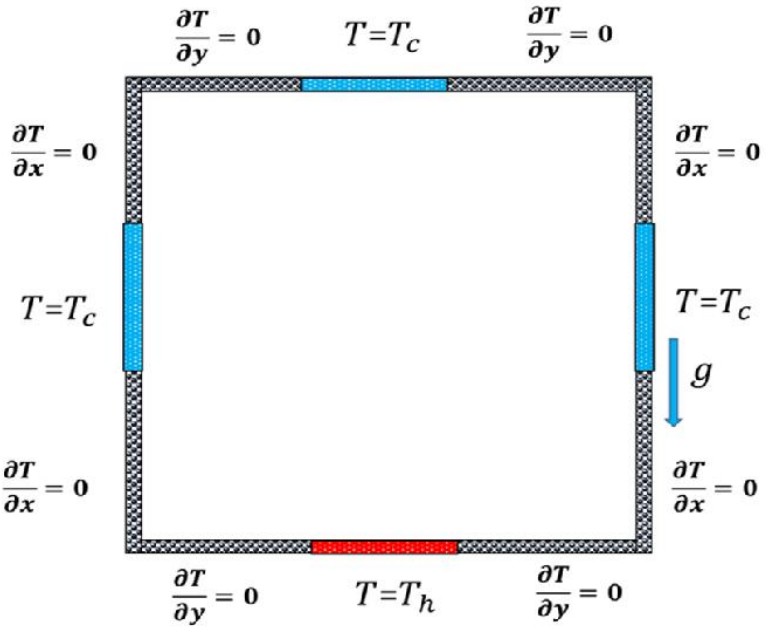


Fig. 1 Schematic diagram.

Non-Dimensional Variables

$X = \frac{x}{L}; Y = \frac{y}{L}; t = \frac{t^*\alpha_f}{L^2}; U = \frac{uL}{\alpha_f}; V = \frac{vL}{\alpha_f}; P = \frac{p}{\rho_{hnf}\alpha_f^2}; \theta = \frac{T-T_c}{T_h-T_c}; q_{rx} = -\frac{16\sigma T_c^3}{3\beta_T}\frac{\partial T}{\partial x}; \quad q_{ry} = -\frac{16\sigma T_c^3}{3\beta_T}\frac{\partial T}{\partial y}.$

Non-Dimensional form

$$\frac{\partial U}{\partial X} + \frac{\partial V}{\partial Y} = 0 \qquad (5)$$

$$\frac{\partial U}{\partial t} + U\frac{\partial U}{\partial X} + V\frac{\partial U}{\partial Y} = -\frac{\partial P}{\partial X} + \left(\frac{\nu_{hnf}}{\nu_f}\right)Pr\;\left[\frac{\partial^2 U}{\partial X^2} + \frac{\partial^2 U}{\partial Y^2}\right]$$

$$-\left(\frac{\nu_{hnf}}{\nu_f}\right)\frac{Pr}{Da}U+\left(\frac{\sigma_{hnf}}{\sigma_f}\right)\left(\frac{\rho_f}{\rho_{hnf}}\right)Ha^2\ Pr(V\ sin\ sin\ \delta\ \ cos\ cos\ \delta\ -U\ sin^2\ \delta) \quad (6)$$

$$\frac{\partial V}{\partial t}+U\frac{\partial V}{\partial X}+V\frac{\partial V}{\partial Y}=-\frac{\partial P}{\partial Y}+\left(\frac{\nu_{hnf}}{\nu_f}\right)Pr\left[\frac{\partial^2 V}{\partial X^2}+\frac{\partial^2 V}{\partial Y^2}\right]-\left(\frac{\nu_{hnf}}{\nu_f}\right)\frac{Pr}{Da}V$$

$$+\left(\frac{\sigma_{hnf}}{\sigma_f}\right)\left(\frac{\rho_f}{\rho_{hnf}}\right)Ha^2\ Pr\ (U\ sin\ sin\ \delta\ \ cos\ cos\ \delta\ -V\ cos^2\ \delta)+\frac{(\rho\beta)_{hnf}}{\rho_{hnf}\beta_f}\ Pr\ Ra\ \theta \quad (7)$$

$$\frac{\partial\theta}{\partial t}+U\frac{\partial\theta}{\partial X}+V\frac{\partial\theta}{\partial Y}=\left(\frac{\alpha_{hnf}}{\alpha_f}\right)\left[\frac{\partial^2\theta}{\partial X^2}+\frac{\partial^2\theta}{\partial Y^2}\right]\left(1+\frac{4}{3}\frac{k_f}{k_{hnf}}Rd\right)+\left(\frac{\alpha_{hnf}}{\alpha_f}\right)Q\theta \quad (8)$$

Table 1. Physical attributes of Al_2O_3-Cu - MWCNT/water [34].

	Properties of the Ternary Hybrid Nanofluid
Nanoparticles concentration	$\phi=\phi_{p1}+\phi_{p2}+\phi_{p3}$
Density (ρ)	$\rho_{hnf}=(1-\phi_{p1})\left[(1-\phi_{p2})\left[(1-\phi_{p3})\rho_f+\phi_{p3}\rho_{p3}\right]+\phi_{p2}\rho_{p2}\right]+\phi_{p1}\rho_{p1}$
Dynamic viscosity (μ)	$\mu_{thnf}=\frac{\mu_f}{(1-\phi_{p1})^{2.5}(1-\phi_{p2})^{2.5}(1-\phi_{p3})^{2.5}}$
Thermal conductivity (k)	$\frac{k_{thnf}}{k_{hnf}}=\frac{k_{p1}+2k_{hnf}-2\phi_{p1}(k_{hnf}-k_{p1})}{k_{p1}+2k_{hnf}+\phi_{p1}(k_{hnf}-k_{p1})}$ $\frac{k_{hnf}}{k_{nf}}=\frac{k_{p2}+2k_{nf}-2\phi_{p2}(k_{nf}-k_{p2})}{k_{p2}+2k_{nf}+\phi_{p2}(k_{nf}-k_{p2})}$ $\frac{k_{nf}}{k_f}=\frac{k_{p3}+2k_f-2\phi_{p3}(k_f-k_{p3})}{k_{p3}+2k_f+\phi_{p3}(k_f-k_{p3})}$
Thermal volume capacity (ρC_p)	$(\rho C_p)_{thnf}=(1-\phi_{p1})\left[(1-\phi_{p2})\left[(1-\phi_{p3})(\rho C_p)_f+\phi_{p3}(\rho C_p)_{p3}\right]+\phi_{p2}(\rho C_p)_{p2}\right]+\phi_{p1}(\rho C_p)_{p1}$
Thermal expansion ($\rho\beta$)	$(\rho\beta)_{thnf}=(1-\phi_{p1})\left[(1-\phi_{p2})\left[(1-\phi_{p3})(\rho\beta)_f+\phi_{p3}(\rho\beta)_{p3}\right]+\phi_{p2}(\rho\beta)_{p2}\right]+\phi_{p1}(\rho\beta)_{p1}$
Thermal diffusivity (α)	$\alpha_{thnf}=\frac{k_{thnf}}{(\rho C_P)_{thnf}}$
Electrical conductivity (σ)	$\frac{\sigma_{thnf}}{\sigma_{hnf}}=1+\left[\frac{3\left(\frac{\sigma_{p1}}{\sigma_{hnf}}-1\right)\phi_{p1}}{\left(\frac{\sigma_{p1}}{\sigma_{hnf}}+2\right)-\left(\frac{\sigma_{p1}}{\sigma_{hnf}}-1\right)\phi_{p1}}\right]$ $\frac{\sigma_{hnf}}{\sigma_{nf}}=1+\left[\frac{3\left(\frac{\sigma_{p2}}{\sigma_{nf}}-1\right)\phi_{p2}}{\left(\frac{\sigma_{p2}}{\sigma_{nf}}+2\right)-\left(\frac{\sigma_{p2}}{\sigma_{nf}}-1\right)\phi_{p2}}\right]$ $\frac{\sigma_{nf}}{\sigma_f}=\left[1+\frac{3\left(\frac{\sigma_{p3}}{\sigma_f}-1\right)\phi_{p3}}{\left(\frac{\sigma_{p3}}{\sigma_f}+2\right)-\left(\frac{\sigma_{p3}}{\sigma_f}-1\right)\phi_{p3}}\right]$

Heat transfer coefficient

$$h_{hnf}=\frac{q}{T_h-T_c}$$

Heat flux

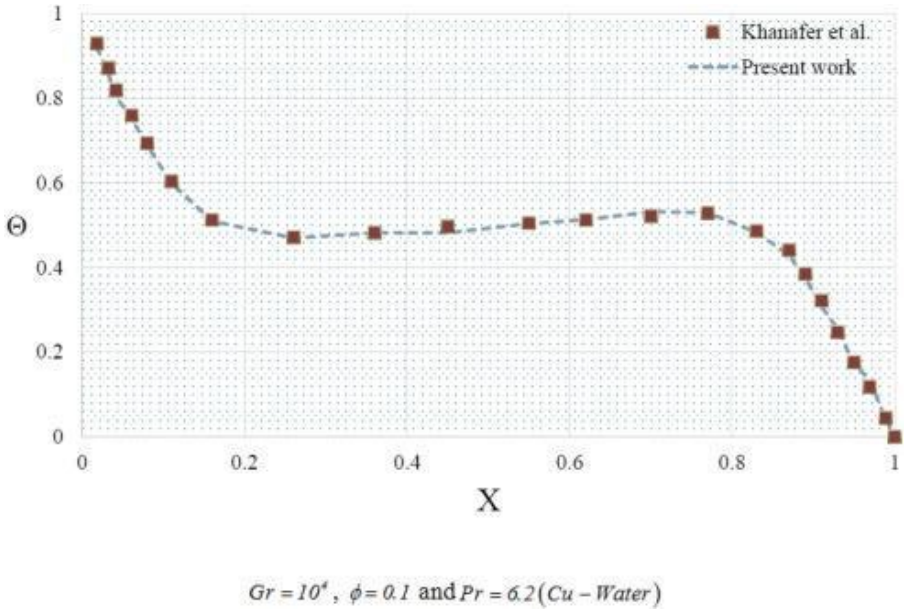
$$q = -k_{hnf} \frac{T_h - T_c}{L} \frac{\partial \theta}{\partial n}$$

Nusselt number

$$Nu = \left(\frac{k_{hnf}}{k_f}\right)\left(1 + \frac{4}{3} Rd \left(\frac{k_{hnf}}{k_f}\right)^{-1}\right)\frac{\partial \theta}{\partial Y}$$

The average Nusselt number on hot wall is gained from the resulting relation

$$Nu_{avg} = \frac{1}{L}\int_L \quad Nu\, dX$$



$Gr = 10^4$, $\phi = 0.1$ and $Pr = 6.2 (Cu - Water)$

Fig. 2. Code testing considering data of Ref. [27].

To validate the accuracy of the model, a benchmark case involving free convection was employed, as illustrated in Fig. 2, which demonstrates the strong agreement between the simulation results and recognized reference data. In this validation, a hybrid nanofluid composed of MWCNT and Fe_3O_4 nanoparticles dispersed in water was utilized, capitalizing on the enhanced thermal properties that result from the synergistic possessions of these nanoparticles. The incorporation of this hybrid nanomaterial significantly improved the thermal performance of the base fluid, confirming the robustness and reliability of the modeling approach. To evaluate the exactness and reliability of the present numerical model, a benchmark study of free convection was conducted using reference data [27]. The validation results, depicted in Fig. 2, confirm the high accuracy and

correctness of the computational approach. In this validation test, free convection of a copper oxide water nanofluid was simulated, and the obtained results showed excellent agreement with benchmark data, thereby verifying the numerical framework. For the current study, the simulation incorporates a ternary hybrid nanofluid, consisting of MWCNTs, copper, and Al_2O_3 dispersed in water. The inclusion of these hybrid nanoparticles enhances the thermo-physical properties of the base fluid, resulting in a new fluid with superior thermal conductivity, modified viscosity, and improved convective energy transfer characteristics. The successful validation of the model against benchmark data confirms its suitability for investigating free convection in a permeable enclosure under the impact of an inclined magnetic field, *Rd*, and internal *Q*.

3. NUMERICAL METHOD

Numerical simulation of free convection in a porous enclosure filled with a ternary hybrid nanofluid is performed via the MAC method. This approach is well-suited for solving incompressible fluid flow problems and is employed here to discretize the equations for continuity, momentum, and energy. The computational domain is designed with a uniform grid, where pressure is stored at cell centers, velocity components at cell faces, and temperature at cell centers. No-slip velocity conditions are useful at all walls, while thermal boundary conditions consist of a centrally heated bottom wall, a centrally cooled top wall, and adiabatic sidewalls. A uniform grid spacing ($\Delta x=\Delta y$) is used for spatial discretization, and the time-stepping method ensures stability and convergence. The computational domain is a staggered grid, ensuring stability and accurate treatment of pressure-velocity coupling. The MAC method involves the following key steps:

a) Velocity prediction using the momentum equations (without pressure).
b) Pressure correction to enforce the incompressibility constraint via the pressure Poisson equation.
c) Velocity correction to satisfy the divergence-free condition.
d) Temperature updates using the energy equation.

These equations are discretized using the FDM, and the resulting algebraic equations are solved iteratively until convergence is achieved.

Table 2. Thermal physical Properties of water and nanoparticles [33].

Property	H_2O	Al_2O_3	Cu	$MWCNT$
$\rho(\mathrm{kg}m^{-3})$	997.1	3970	8933	1600
$C_p(\mathrm{J}kg^{-1}K^{-1}$	4179	765	385	796
$\mathrm{k}(\mathrm{W}m^{-1}k^{-1})$	0.613	40	401	3000
$\beta(K^{-1})$	21×10^{-5}	0.85×10^{-5}	1.67×10^{-5}	4.2×10^{-5}
$\sigma(\Omega^{-1}m^{-1})$	0.05	1×10^{-10}	5.96×10^{7}	4.8×10^{-7}
μ (Pa s)	8.9×10^{-4}	-	-	-
Pr	6.2	-	-	-

4. RESULTS AND PHYSICAL MECHANISM BEHIND

The numerical investigation explores the possessions of key parameters, including the *Ra*, *Da*, *Ha*, *Rd*, and heat generation/absorption parameter (Q) on the free convection behavior of a ternary *hnf* in a porous enclosure. The outcomes are analyzed in terms of streamlines, isotherms, velocity distributions, and *Nu* variations to evaluate the impact of these parameters on heat transfer characteristics.

Figures 3 and 4 illustrate the result of *Ra* over streamlines and isotherms, respectively, for *Ha=2, Da=0.1, Rd =1,* and heat generation*=0.5*. At lower *Ra*, the flow is feeble, and conduction dominates energy transfer, as seen from the nearly parallel isotherms and weak circulations in the streamlines. As Ra increases, buoyancy-driven convection intensifies, forming stronger circulation cells that transport heat more effectively. The thinning of the thermal boundary layer near the heated bottom region indicates greater convective heat transfer. The transition from conduction-dominant ($Ra = 10^3$) to convection-dominant ($Ra = 10^6$) flow is evident, as higher *Ra* strengthens the fluid motion, promoting efficient heat transfer.

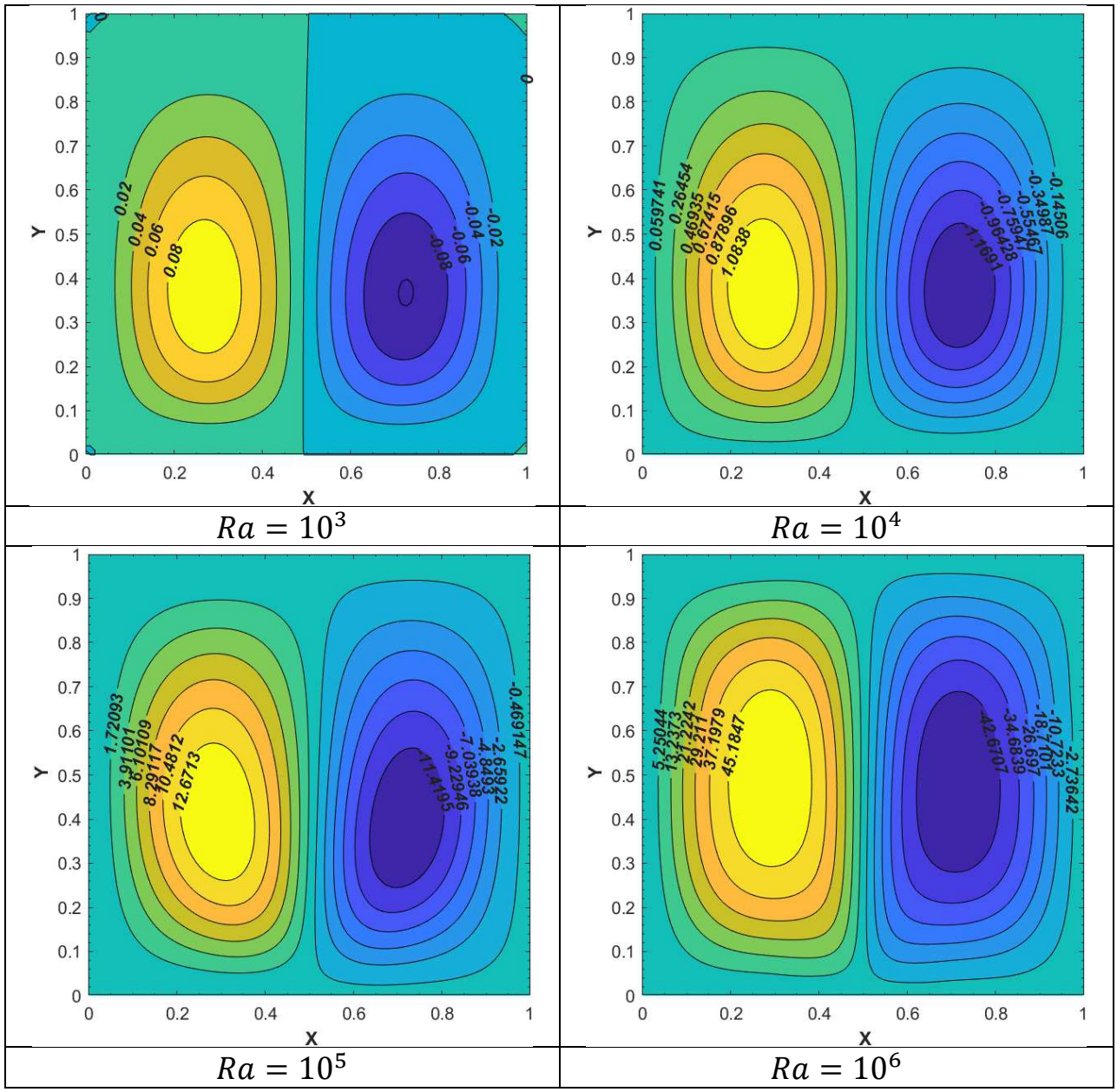


Fig. 3 The influence of Ra on streamlines for Ha =2, Da = 0.1, Rd = 1 and Q = 0.5.

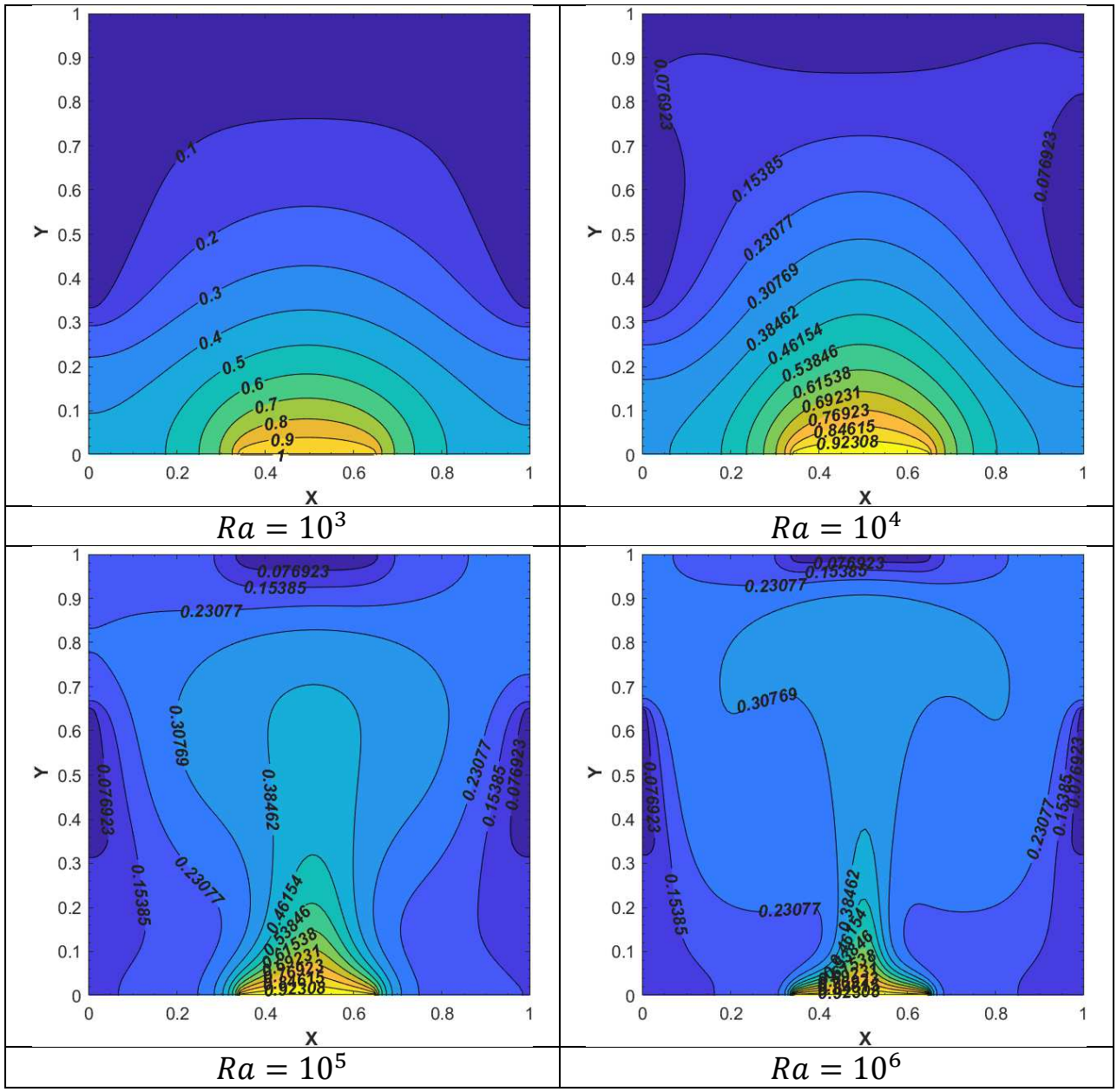


Fig. 4 The influence of Ra on isotherms for Ha =2, Da = 0.1, Rd = 1 and Q = 0.5.

Figures 5 and 6 depict the impact of the *M* on isotherms and streamlines for Ha=0, 10, 30, 50 while keeping Da=0.1, Rd =1, and Q=0.5 constant. At Ha=0, the nonappearance of the Lorentz

force allows strong convective currents, leading to well-developed circulations and enhanced energy transfer. However, as *Ha* rises, the applied magnetic field generates a Lorentz force that resists the motion of the conducting fluid, suppressing the buoyancy-driven flow. This suppression leads to a reduction in vortex strength, causing the streamlines to shrink and become less pronounced.

The permeability of the permeable medium, represented by the Darcy number, significantly affects the flow and energy transfer characteristics, as shown in **Figures 7 and 8** for Da=0.1,0.01,0.001,0.0001 with Ha=2, Rd =1, and Q=0.5. For high permeability *(Da*=0.1), the porous medium offers minimal resistance, allowing strong fluid motion and well-defined convective cells. However, as *Da* decreases, the increased flow resistance dampens the strength of convection currents, restricting fluid circulation. At very low permeability (Da=0.0001), flow is almost completely suppressed, resulting in a conduction-dominated regime with weak convective effects. This transition is evident from the increasing uniformity of isotherms and the weakening of streamlines.

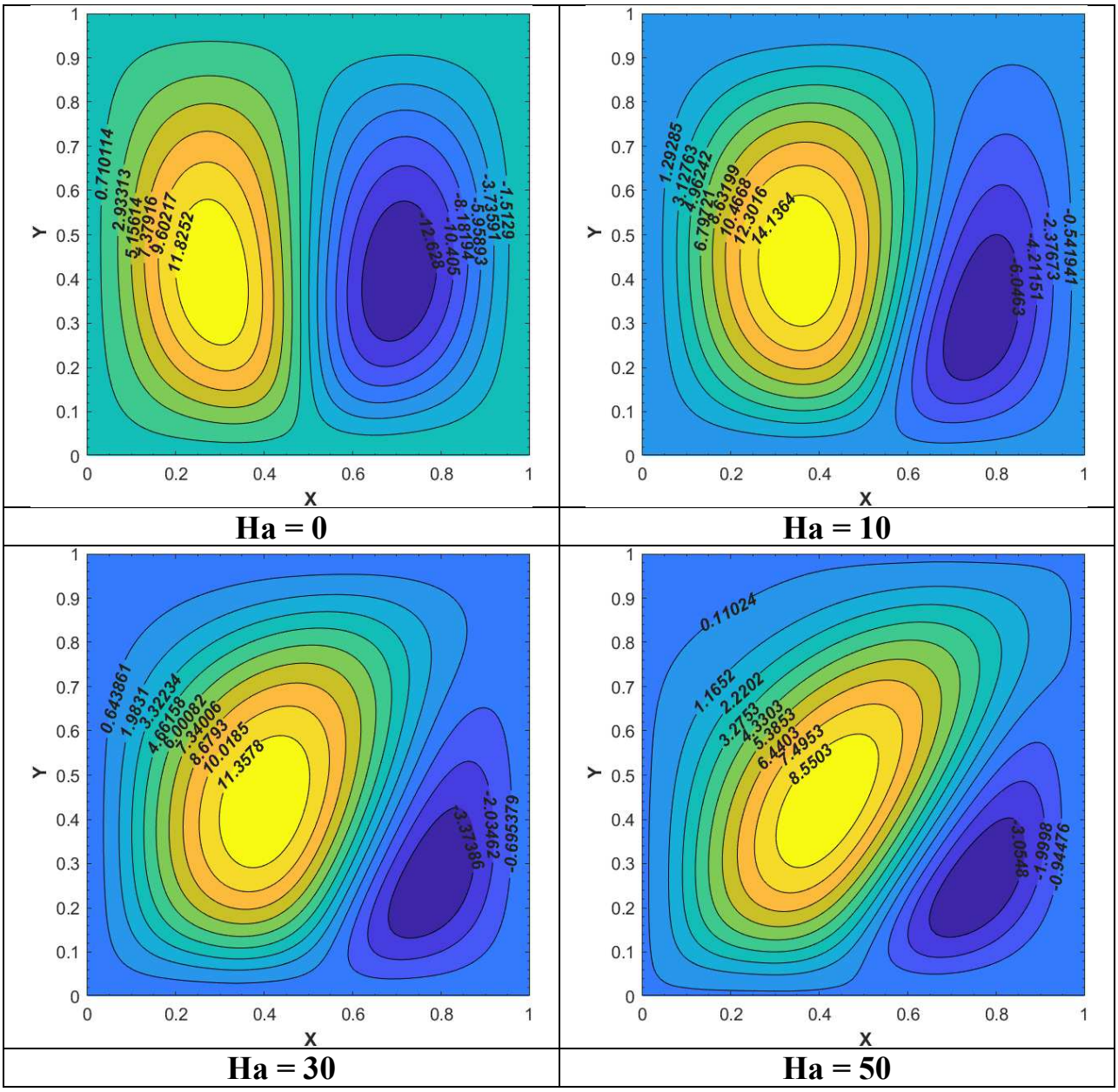


Fig. 5 The influence of Ha on streamlines for $Ra = 10^5$, Da = 0.1, Rd = 1 and Q = 0.5.

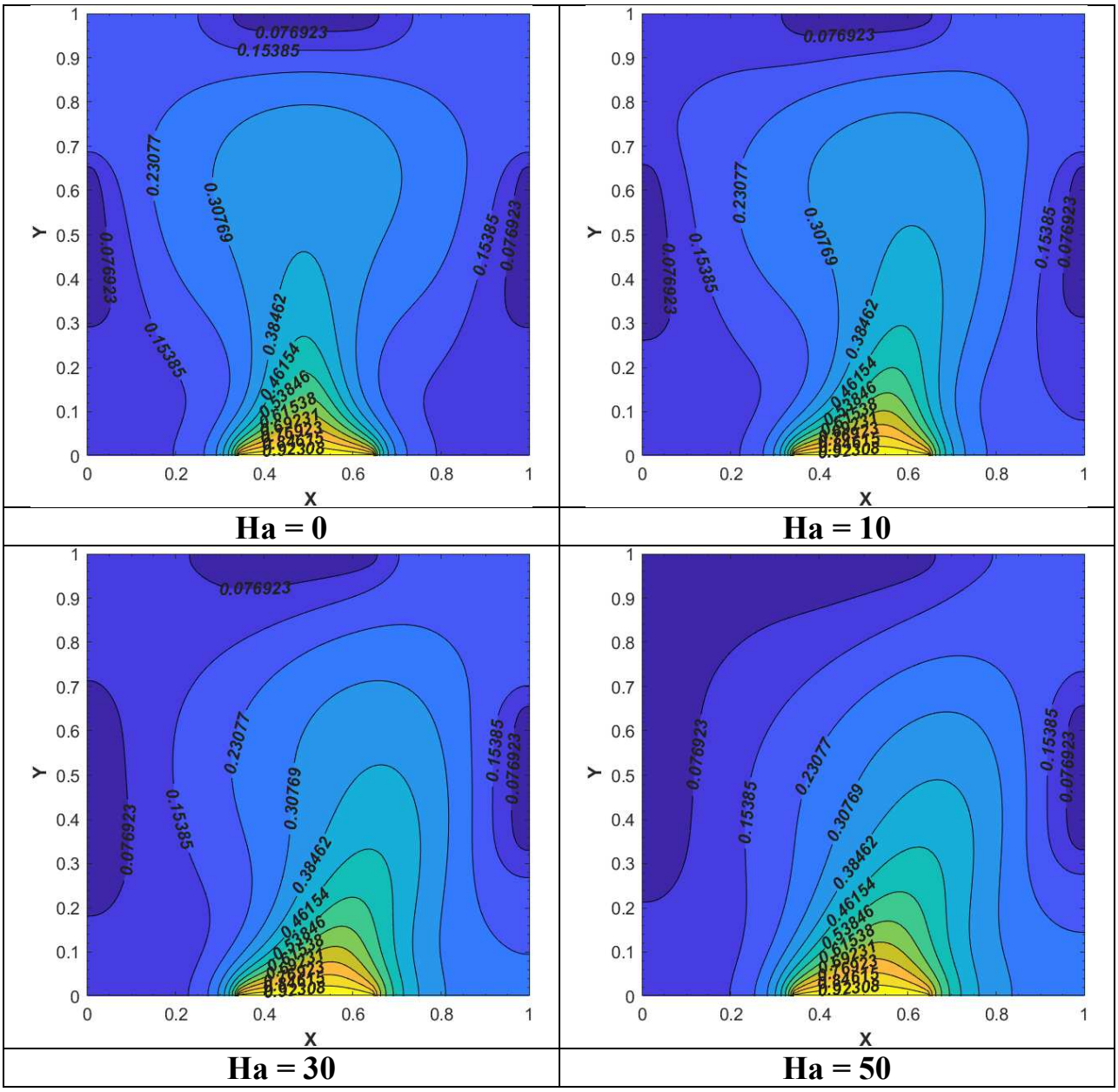


Fig. 6 The influence of Ha on isotherms for $Ra = 10^5$, Da = 0.1, Rd = 1 and Q = 0.5.

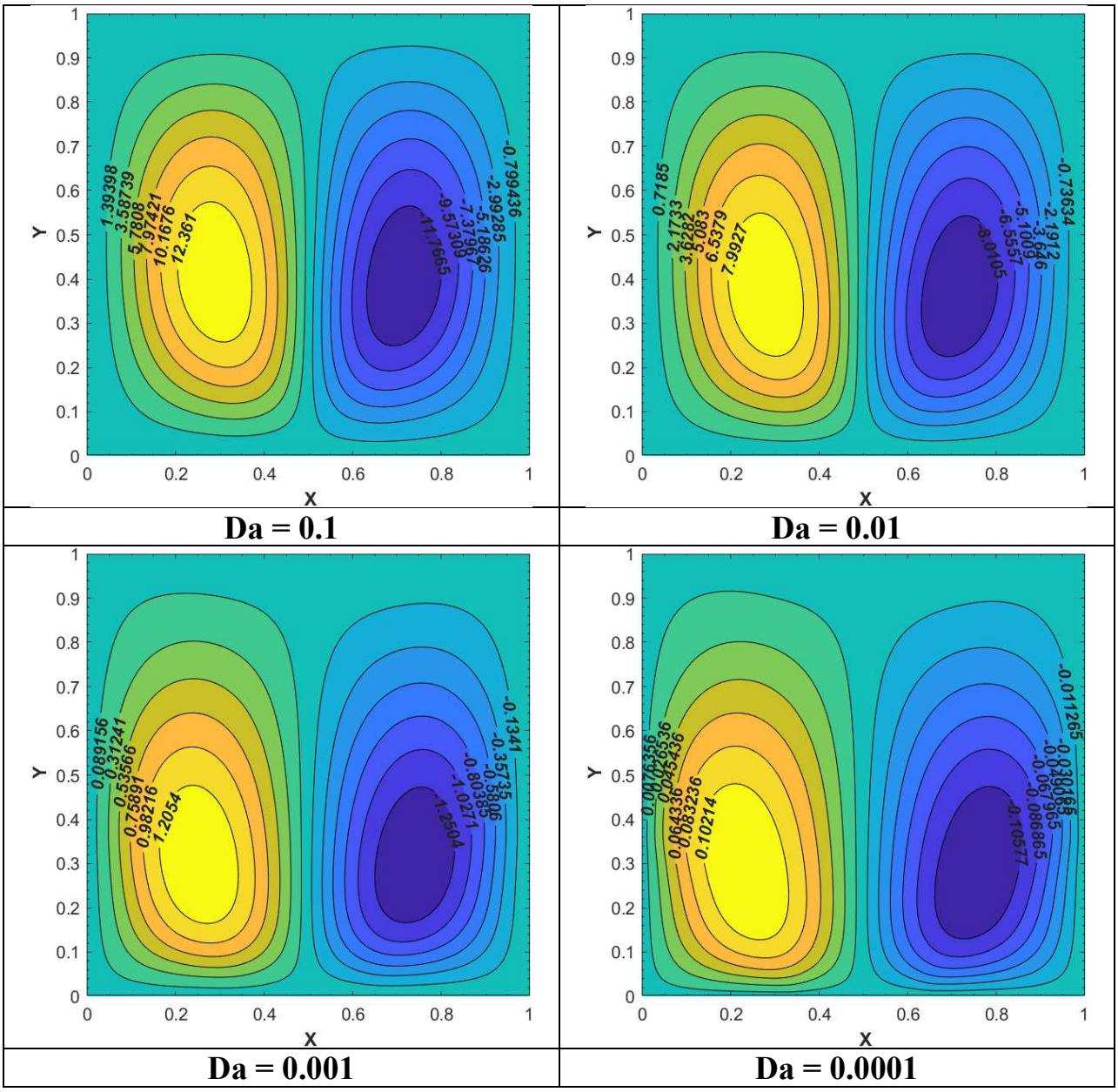


Fig. 7 The influence of Da on streamlines for $Ra = 10^5$, Ha = 2, Rd = 1 and Q = 0.5.

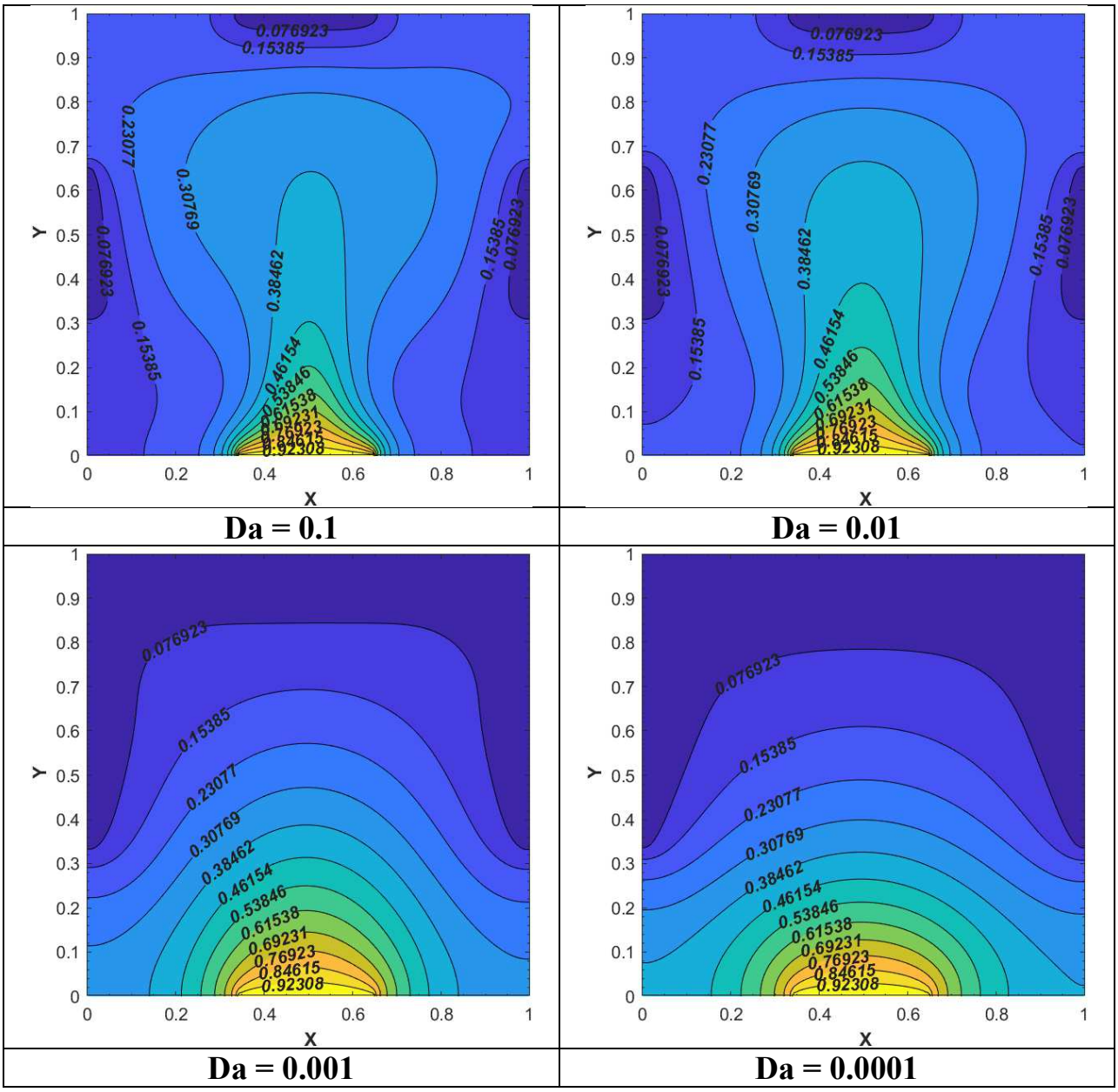


Fig. 8 The influence of Da on isotherms for $Ra = 10^5$, Ha = 2, Rd = 1 and Q = 0.5.

Figures 9 and 10 show the impact of *Rd* on streamlines and isotherms for Rd =0, 1, 3, 5 while maintaining *Ha=2, Da=0.1, and Q=0.5*. For low radiation levels (*Rd* = 0), convection remains the dominant heat transfer mode, as seen from well-defined vortices and significant temperature

gradients. As *Rd* increases, heat transfer enhances thermal energy transport, causing isotherms to become more uniform and reducing the temperature gradient. At *Rd* =5, radiation dominates the heat transfer process, leading to enhanced heat distribution and a higher Nusselt number.

The result of internal heat generation or absorption is shown in **Figures 11 and 12** for Q=0, 1, 3, 5 with *Ha=2, Rd =1.0 and Da=0.1*. At *Q=0*, the natural convection remains unaltered. However, as *Q* increases, the internal heat source contributes additional energy to the system, leading to an increase in overall fluid temperature. This effect reduces the temperature gradient, thereby weakening buoyancy-driven convection and reducing the strength of flow circulations. Consequently, the energy transfer rate declines, as shown in Figure 18, where the Nu_a decreases with increasing *Q*. This trend suggests that excessive internal heat generation can act as a thermal barrier, reducing convection efficiency. Conversely, in heat absorption cases (Q<0), stronger convective motions enhance the heat transfer process.

Figure 13 examines the impact of the inclination angle of the *M* on the *Nu* along the bottom heat source for *Ha=2, Da=0.1, Q=0.5, and Rd =1.0*. As the orientation of the magnetic field changes, the suppression of free convection varies, leading to different heat transfer distributions. When the *M* is aligned with the flow, convective motion is more suppressed, reducing heat transfer. However, at certain angles, the damping effect of the magnetic force weakens, allowing convection to persist. This suggests that adjusting the inclination angle of the *M* can be a potential control mechanism for optimizing energy transfer in MHD-driven natural convection systems.

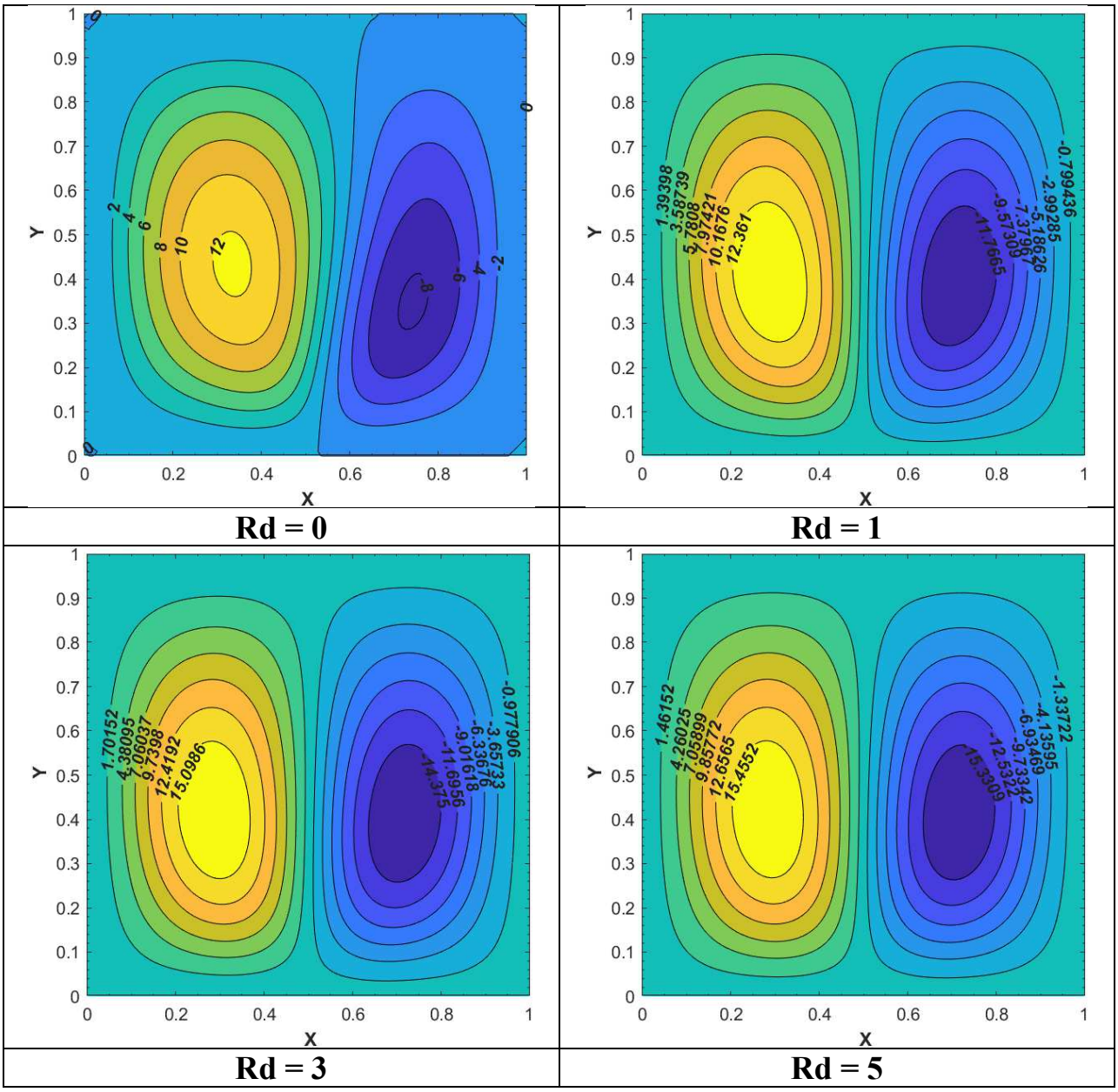


Fig. 9 The influence of Rd on streamlines for $Ra = 10^5$, Ha = 2, Da = 0.1 and Q = 0.5.

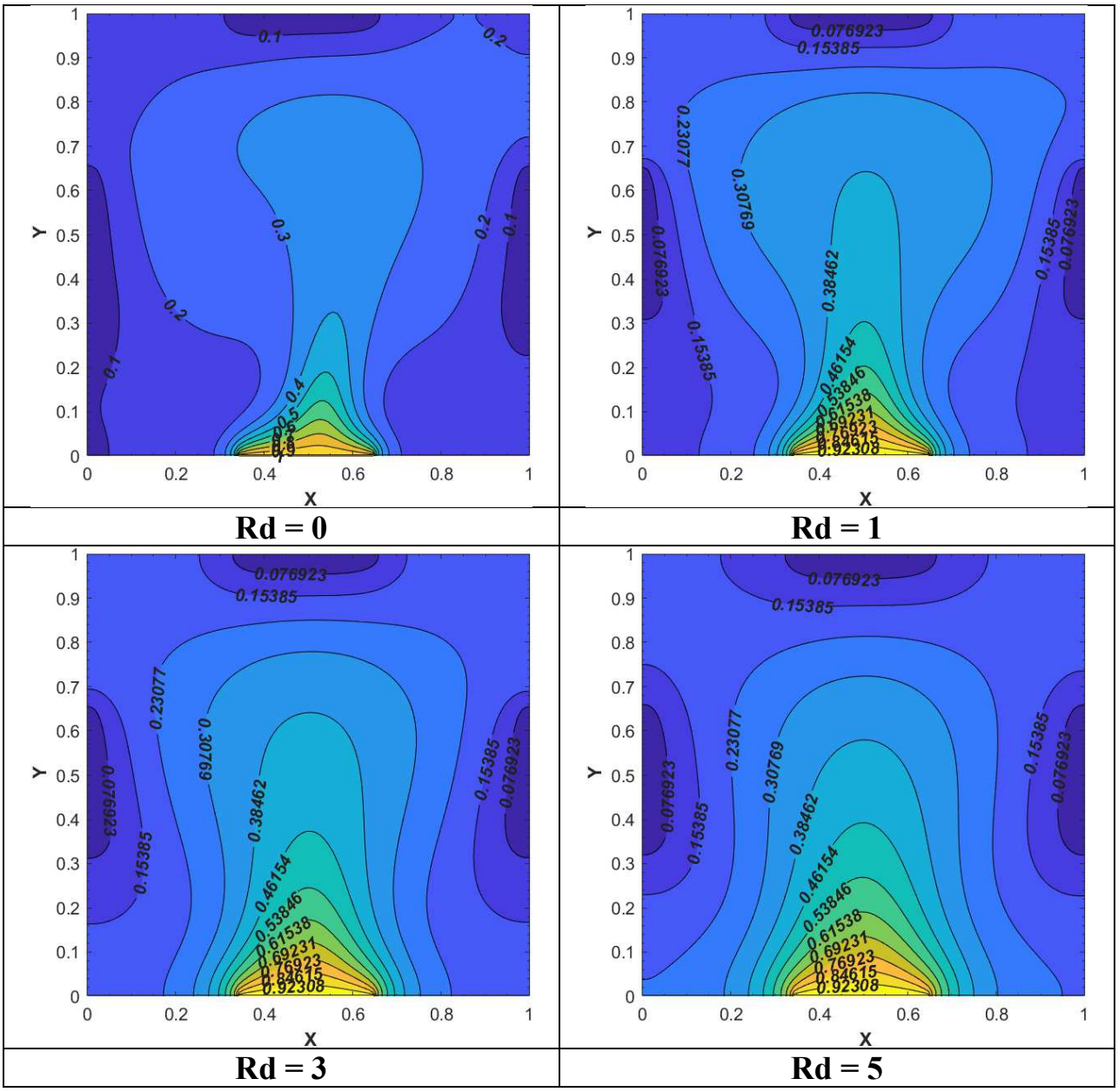


Fig. 10 The influence of Rd on isotherms for $Ra = 10^5$, Ha = 2, Da = 0.1 and Q = 0.5.

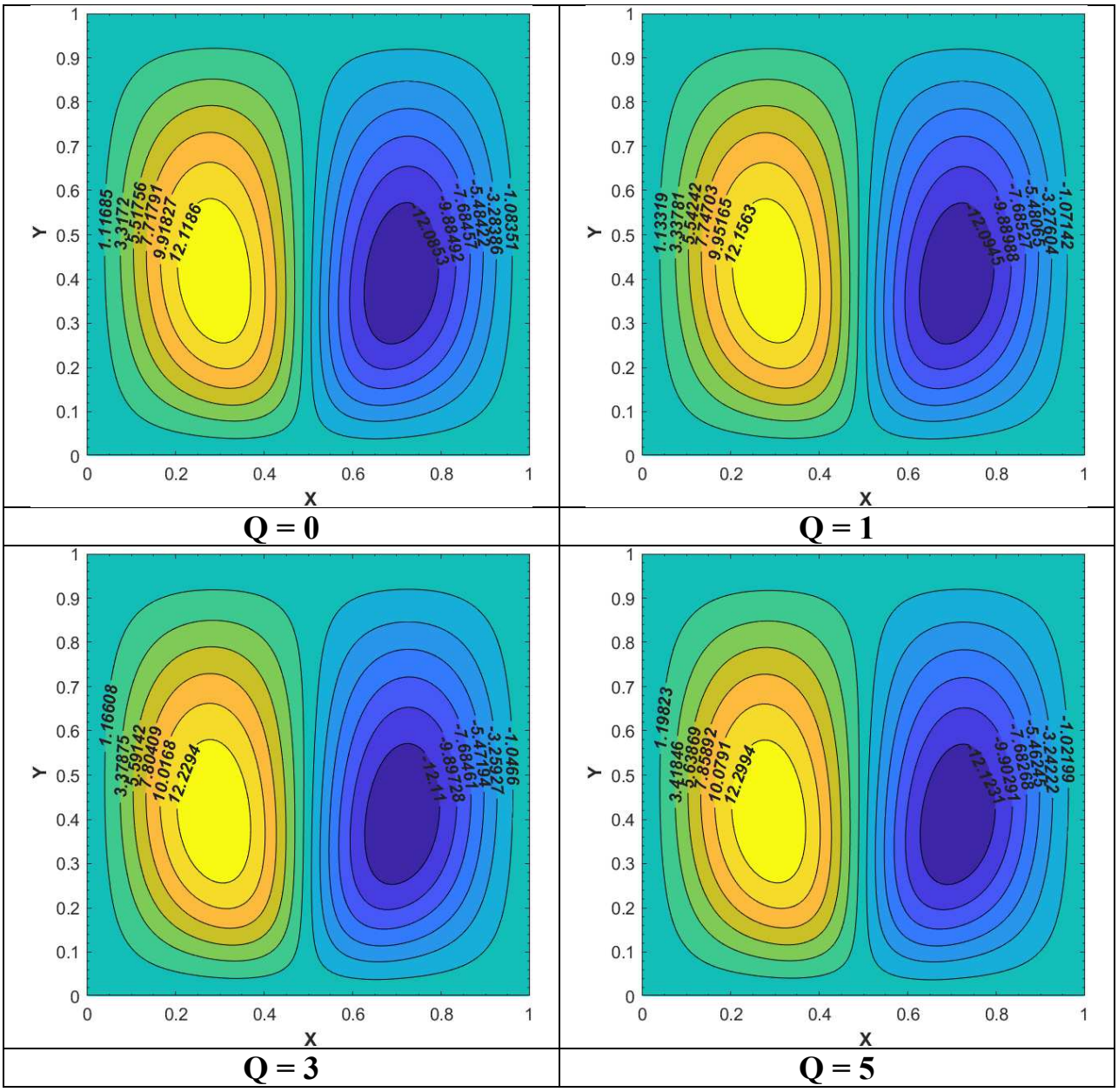


Fig. 11 The influence of Q on streamlines for$Ra = 10^5$, Ha = 2, Da = 0.1 and Rd = 1.0.

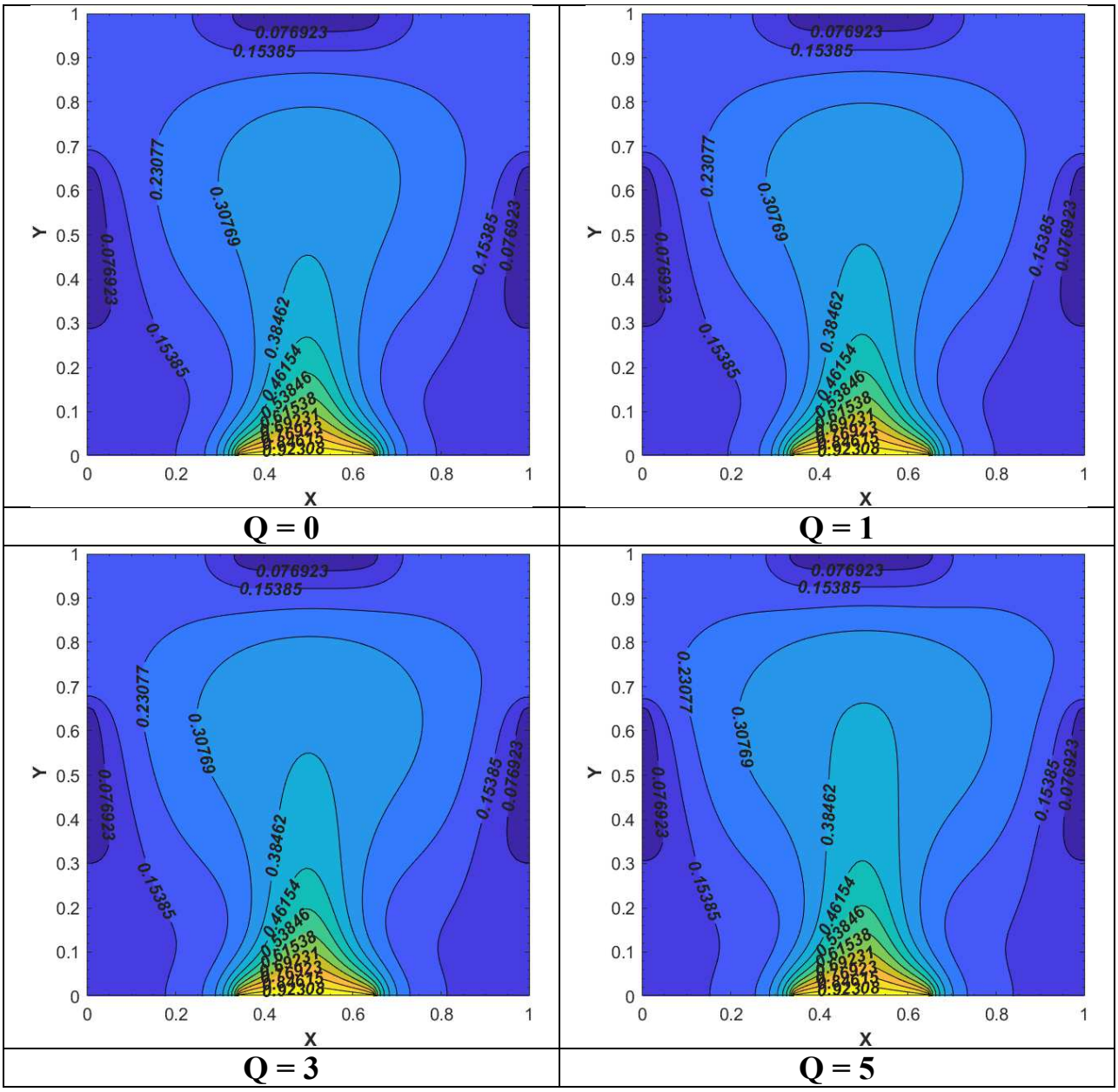


Fig. 12 The influence of Q on isotherms for$Ra = 10^5$, Ha = 2, Da = 0.1 and Rd = 1.0.

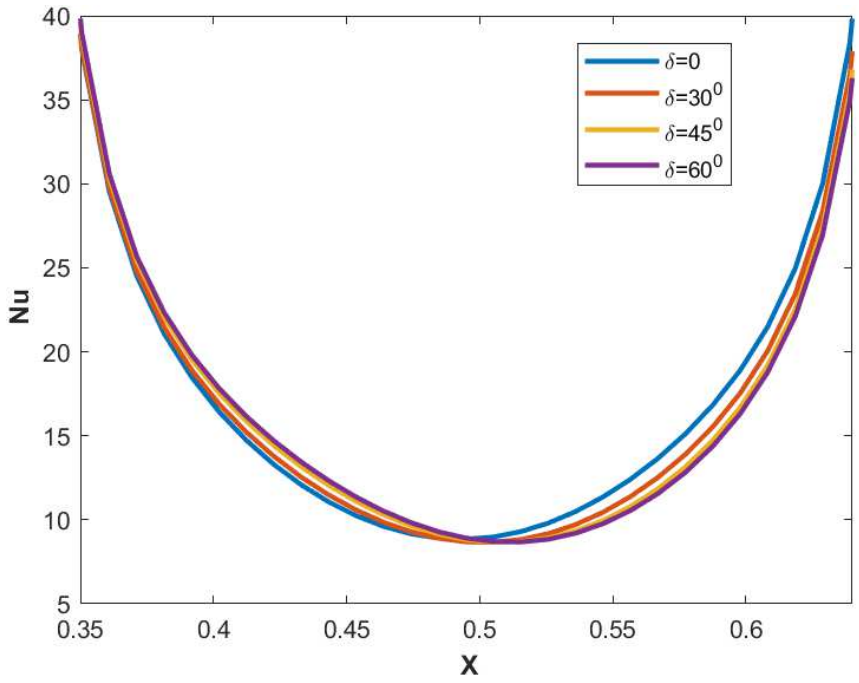


Fig. 13 The influence of magnetic field orientation angle δ on local Nusselt number along the heat source on bottom wall with $Ra = 10^5$, Ha = 2, Da = 0.1, Q = 0.5 and Rd = 1.0

Figure 14 shows that the Nu_a surges with increasing *Rd*, confirming the role of radiation in enhancing heat transport. The results indicate that in high-temperature applications, where radiative heat transfer is significant, neglecting *Rd* may lead to an underestimation of heat transfer rates. This is further confirmed by the increase in the Nu_a along the heated bottom surface in **Figure 15**, which shows a significant rise in energy transfer rates as *Ra* surges. The results suggest that at higher *Ra*, convective mixing enhances thermal performance, making natural convection the dominant heat transfer mode.

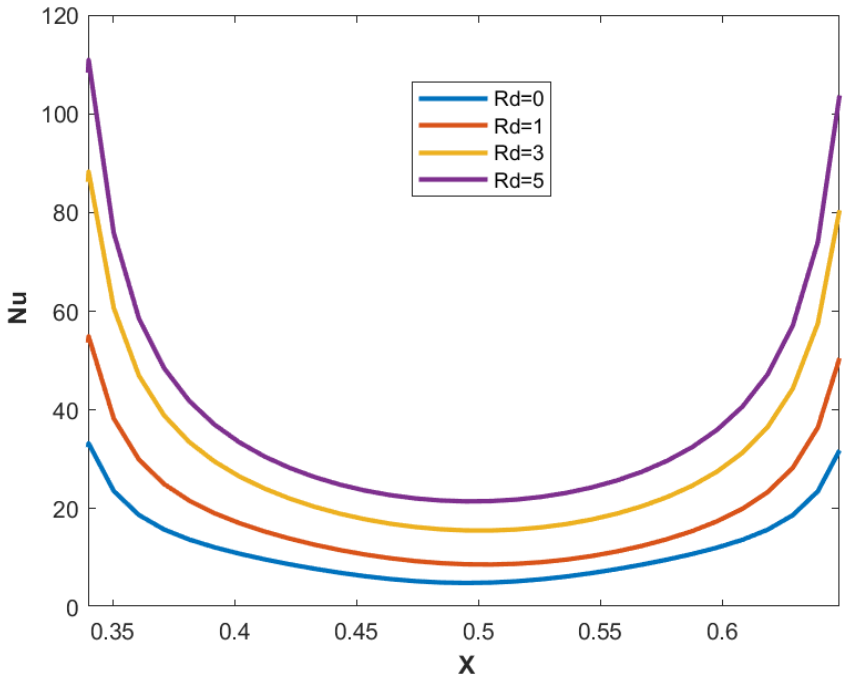


Fig. 14 The influence of radiation Rd on local Nusselt number along the heat source on bottom wall with $Ra = 10^5$, Ha = 2, Da = 0.1, and Q = 0.5.

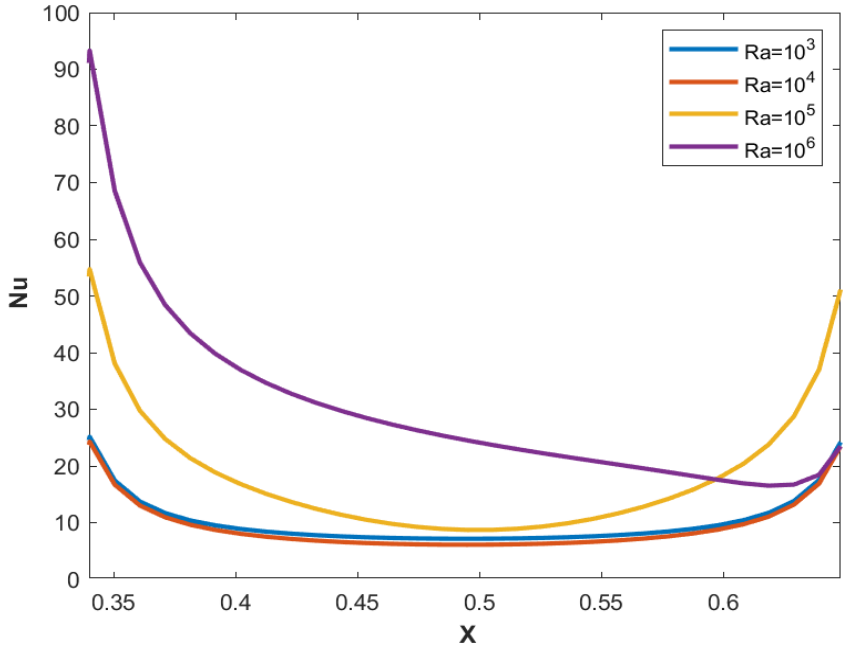


Fig. 15 The influence of Ra on local Nusselt number along the heat source on bottom wall with Rd =, Ha = 2, Da = 0.1, and Q = 0.5.

The corresponding isotherms become more stratified at higher *Ha*, indicating a shift towards conduction-dominant energy transfer. The decrease in convective strength is also reflected in **Figure 16,** where the Nu_a along the heated bottom wall declines with increasing Ha. These results highlight the controlling outcome of the magnetic field in regulating heat transfer, where stronger fields suppress convective motion, reducing heat transport efficiency. Such behavior is particularly useful in applications requiring thermal insulation or controlled heat dissipation under electromagnetic influence. **Figure 17** further confirms this trend, showing a decreasing local Nusselt number as Da decreases, indicating reduced convective contribution. The results suggest that in highly porous media, convection plays a dominant role, whereas in low-permeability systems, heat transfer is primarily controlled by conduction. This behavior is crucial in designing porous structures where either enhanced convection (high Da) or controlled insulation (low *Da*) is desired.

Figure 18 illustrates the influence of key dimensionless parameters *Ra*, *Da*, *Ha*, *Rd*, and *Q* on the Nu_a, which quantifies the energy transfer rate along the heat source on the bottom wall. The results indicate that swelling *Ra* significantly enhances energy transfer due to tougher buoyancy-driven convection, transitioning from a conduction-dominated regime at low *Ra* to a convection-dominated regime at high *Ra*, where well-developed circulation cells improve fluid mixing and thermal transport. Conversely, decreasing *Da* reduces permeability, suppressing convection and lowering u_a, shifting the energy transfer mechanism toward conduction dominance, which is relevant in porous media applications such as geothermal energy and insulation materials. The application of a magnetic field, represented by increasing *Ha*, results in a decline in Nu_a due to the Lorentz force, which dampens convective motion, transforming the system into a conduction-dominant regime, making it useful for electromagnetic heat control applications such as MHD power generators and cooling of nuclear reactors. Thermal radiation, characterized by *Rd*, has the opposite effect, as increasing *Rd* enhances radiative heat transport, leading to a surge in Nu_a by supplementing convective and conductive heat transfer, making radiation an essential factor in high-temperature applications like solar collectors and aerospace thermal systems. Additionally, increasing *Q* (internal heat generation) weakens natural convection by reducing the temperature gradient, thereby lowering Nu_a , which is crucial in applications like nuclear reactor cooling, thermal energy storage, and electronic device heat dissipation, whereas heat absorption enhances convection and increases Nu_a. These findings emphasize the complex

interplay between natural convection, magnetic damping, porous resistance, radiative effects, and heat generation, providing crucial insights into optimizing heat transfer performance in engineering applications, including industrial heat exchangers, electronic cooling systems, and thermal management in energy storage technologies.

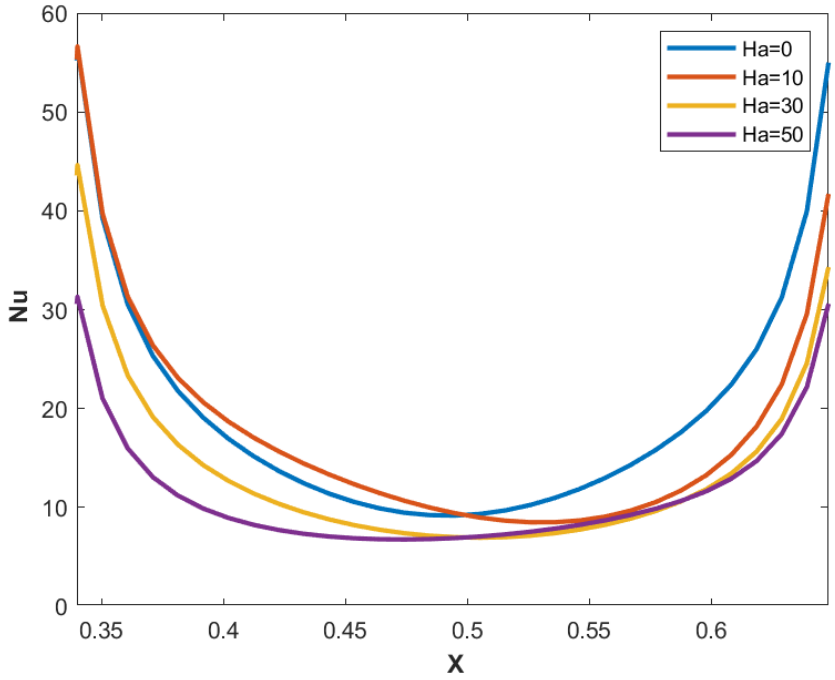


Fig. 16 The influence of Ha on local Nusselt number along the heat source on bottom wall with $Ra = 10^5$, Rd = 1.0, Da = 0.1, and Q = 0.5.

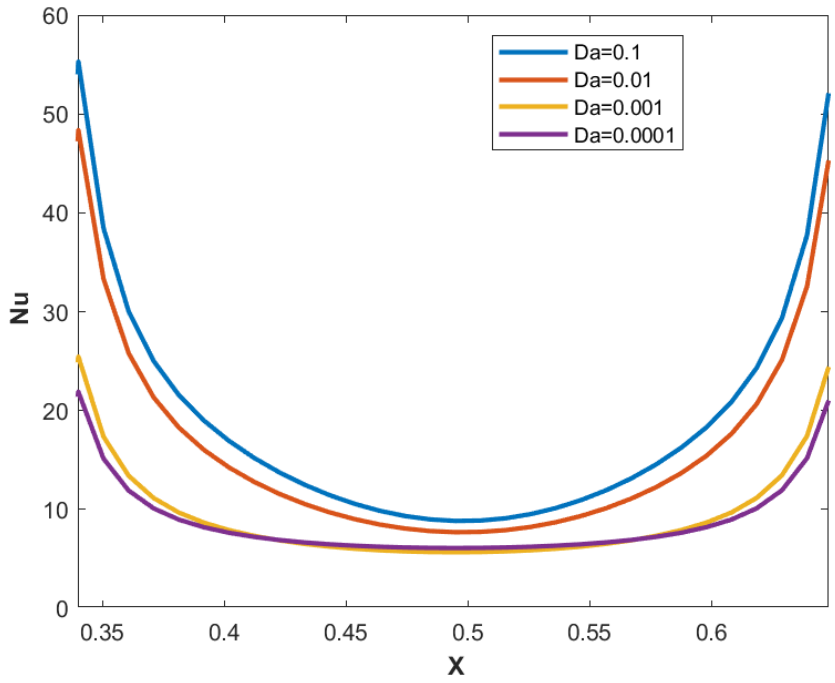


Fig. 17 The influence of Da on local Nusselt number along the heat source on bottom wall with $Ra = 10^5$, Ha = 2, Rd = 1, and Q = 0.5.

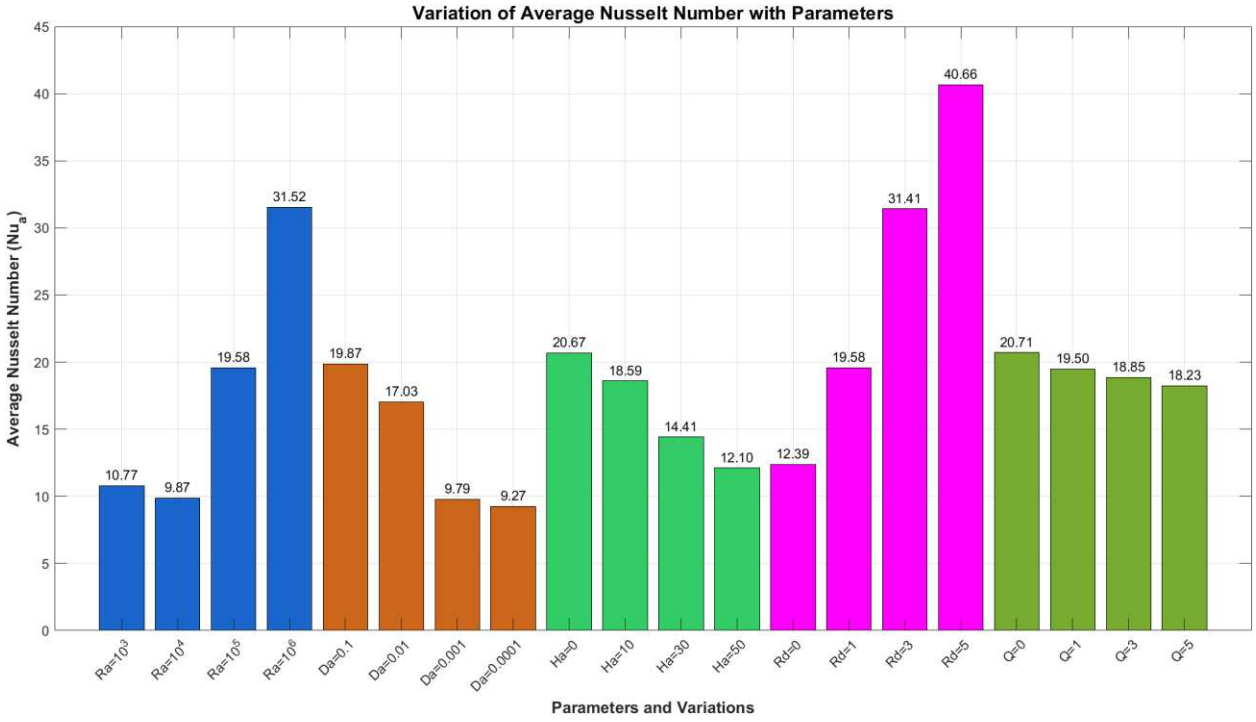


Fig. 18 The influence of key parameters on the average Nusselt number along the heat source on the bottom wall.

5. CONCLUSION

This study comprehensively investigates the free convection of a ternary hybrid nanofluid in a permeable enclosure under the combined effects of an inclined magnetic field, thermal radiation, and heat generation using the MAC method. The results provide significant insights into the thermal behavior of hybrid nanofluids in permeable media and quantify the impact of various dimensionless parameters on heat transfer rates. Key observations indicate that increasing the *Ra* from $10^3 to\ 10^6$ enhances convective energy transfer, leading to a 192% increase in the average *Nu* due to the intensification of buoyancy-driven fluid motion. Reducing the *Da* from 0.1 to 0.0001 suppresses convective heat transfer, causing a 53% drop in Nu_a as the porous medium restricts fluid circulation and transitions the system toward a conduction-dominated regime. The application of an *Ha* from 0 to 50 significantly reduces heat transfer efficiency, with the Nusselt number decreasing by 41%, confirming the damping effect of the Lorentz force on convective motion. Conversely, increasing the thermal radiation parameter (Rd) from 0 to 5 leads to a 229% enhancement in Nu_a, demonstrating the substantial contribution of radiative heat transfer in high-temperature applications. The occurrence of Q weakens natural convection by reducing the temperature gradient, leading to a 12% decrease in heat transfer for Q=5, while heat absorption enhances convection and increases the Nusselt number.

The results demonstrate that proper tuning of these parameters is crucial for optimizing energy transfer performance in permeable media applications. These findings have direct implications for engineering systems such as industrial heat exchangers, nuclear reactor cooling, MHD power generation, electronic cooling, solar thermal collectors, and energy storage technologies. Additionally, the study provides valuable insights into how ternary hybrid nanofluids behave under complex thermal and electromagnetic conditions, emphasizing their potential for enhanced heat dissipation and thermal control applications. Overall, this study establishes a solid foundation for future research in the field of MHD free convection in hybrid nanofluids, offering a framework for experimental validation and further numerical refinements. Future work could explore time-dependent effects, three-dimensional configurations, and different nanoparticle combinations to further optimize heat transfer in advanced thermal systems.

Funding
The authors declare that no funds, grants, or other support were received for this study.

Conflict of interest Statement
The authors declare that there is no conflict of interest regarding the publication of this paper.

Data Availability Statement

The data that support the findings of this study are available from the corresponding author upon reasonable request.

References

[1] C. C. Cho et al., "Natural convection heat transfer performance in complex-wavy-wall enclosed cavity filled with nanofluid," Int. J. Therm. Sci., vol. 60, pp. 255–263, 2012.

[2] P. Mondal et al., "MHD double-diffusive mixed convection and entropy generation of nanofluid in a trapezoidal cavity," Int. J. Mech. Sci., vol. 15, p. 208, 2021.

[3] H. Kim et al., "Computational analysis of magnetohydrodynamic ternary-hybrid nanofluid flow and heat transfer inside a porous cavity with shape effects," Phys. Fluids, vol. 36, no. 8, 2024.

[4] M. Sheikholeslami and S. A. Shehzad, "Magnetohydrodynamic nanofluid convection in a porous enclosure considering heat flux boundary condition," Int. J. Heat Mass Transf., vol. 106, pp. 1261–1269, 2017.

[5] H. M. Elshehabey et al., "Numerical investigation for natural convection of a nanofluid in an inclined L-shaped cavity in the presence of an inclined magnetic field," Int. Commun. Heat Mass Tran., vol. 57, pp. 228–238, 2014.

[6] N. K. Manna et al., "Effects of enclosure shape on MHD nanofluid flow and irreversibility in different shaped systems under fluid volume constraint," Int. J. Numer. Methods Heat Fluid Flow, vol. 34, no. 2, pp. 666–708, 2024.

[7] N. Z. Khan et al., "A case study on entropy generation in MHD nanofluid flow in L-shaped triangular corrugated permeable enclosure," Case Stud. Therm. Eng., vol. 59, p. 104487, 2024.

[8] M. A. Mansour et al., "MHD effects on entropy generation and heat transfer of nanofluid flows in enclosures," J. Nanofluids, vol. 5, no. 4, pp. 595–605, 2016.

[9] S. A. Mehryan et al., "Free convection of hybrid Al_2O_3-Cu water nanofluid in a differentially heated porous cavity," Adv. Powder Technol., vol. 28, pp. 2295–2305, 2017.

[10] R. S. R. Gorla et al., "Heat source/sink effects on a hybrid nanofluid-filled porous cavity," J. Thermophys. Heat Tran., vol. 31, no. 4, pp. 847–857, 2017.

[11] M. K. Mondal et al., "Assessment of thermal performance of hybrid nanofluid flow in a tilted porous enclosure by imposing partial magnetic fields," Waves Random Complex Media, pp. 1–34, 2022.

[12] Z. Abdel-Nour et al., "Magnetohydrodynamic natural convection of hybrid nanofluid in a porous enclosure: numerical analysis of the entropy generation," J. Therm. Anal. Calorim., vol. 141, pp. 1981–1992, 2020.

[13] V. Rajesh and H. F. Öztop, "Conjugate MHD natural convection in a chamber filled by ternary hybrid nanofluid with entropy generation," Numer. Heat Transfer, Part A, pp. 1–22, 2024.

[14] K. Thirumalaisamy and A. S. Reddy, "Numerical computation on MHD natural convective ternary nanofluid flow and heat transfer in a porous square cavity: Marker-and-cell technique," Int. J. Numer. Methods Heat Fluid Flow, vol. 33, no. 10, pp. 3425–3466, 2023.

[15] S. Munir and Y. U. U. B. Turabi, "Impact of heated wavy wall and hybrid nanofluid on natural convection in a triangular enclosure with embedded cold cylinder under inclined magnetic field," Arab. J. Sci. Eng., pp. 1–14, 2024.

[16] S. Belhaj and B. Ben-Beya, "Thermal performance analysis of hybrid nanofluid natural convection in a square cavity containing an elliptical obstacle under variable magnetic field," Int. J. Numer. Methods Heat Fluid Flow, vol. 32, pp. 1825–1860, 2022.

[17] O. Çiçek et al., "Effect of natural convection hybrid nanofluid flow on the migration and deposition of MWCNT-Fe_3O_4 in a square enclosure," Int. J. Therm. Sci., vol. 190, p. 108318, 2023.

[18] N. C. Roy and I. Pop, "Natural convection of ternary hybrid nanofluid flow in an inclined porous trapezoidal enclosure," J. Eng. Math., vol. 150, no. 1, pp. 1–23, 2025.

[19] B. Souayeh, "Numerical analysis of magnetohydrodynamics mixed convection and entropy generation in a double lid-driven cavity using ternary hybrid nanofluids," Adv. Theory Simul., p. 2401357, 2024.

[20] A. Shafee et al., "Modeling of MHD hybrid nanofluid flow through permeable enclosure," Int. J. Mod. Phys. C, vol. 31, no. 08, p. 2050106, 2020.

[21] M. K. Mondal et al., "Assessment of hybrid nanofluid flow and heat transfer in a porous enclosure with a magnetic field," Waves Random Complex Media, pp. 1–34, 2022.

[22] A. Abdulkadhim et al., "Magnetohydrodynamics hybrid nanofluid in H-wavy enclosure: natural convection and entropy generation," J. Therm. Anal. Calorim., pp. 1–21, 2024.

[23] M. A. Mansour et al., "MHD effects on entropy generation and heat transfer in enclosures containing nanofluids," J. Nanofluids, vol. 5, no. 4, pp. 595–605, 2016.

[24] H. Kim et al., "Computational study of ternary-hybrid nanofluid heat transfer in porous enclosures under MHD effects," Phys. Fluids, vol. 36, no. 8, 2024.

[25] M. Sheikholeslami et al., "Numerical investigation of MHD effects on Al_2O_3–water nanofluid flow and heat transfer in a semi-annulus enclosure using LBM," Energy, vol. 60, pp. 501–510, 2013.

[26] S. Nag et al., "MHD nanofluid heat transport in a corner-heated triangular enclosure at different inclinations," Mater. Today: Proc., vol. 63, pp. 141–148, 2022.

[27] N. Rudraiah, R.M. Barron, M. Venkatachalappa, C.K. Subbaraya, Effect of a magnetic field on free convection in a rectangular enclosure, Int. J. Eng. Sci., 33 (1995), pp. 1075-1084.

[28] Venkatadri, K., Rajarajeswari, P., Anwar Bég, O., Ramachandra Prasad, V., Leonard, H. J., & Kuharat, S. (2025). Thermomagnetic Bioconvection Flow in a Semitrapezoidal

Enclosure Filled With a Porous Medium Containing Oxytactic Micro-Organisms: Modeling Hybrid Magnetic Biofuel Cells. ASME Journal of Heat and Mass Transfer, 147(5).

[29] Venkatadri, K. (2024). Magnetohydrodynamic Natural Convection in a Circular Dome-Shaped Enclosure. Heat Transfer.

[30] Venkatadri, K., Murthy, K. N., Bég, T. A., Bég, O. A., & Kuharat, S. (2024). Numerical simulation of natural convection in a rectangular enclosure filled with porous medium saturated with magnetic nanofluid using Buongiorno's two-component model. The Canadian Journal of Chemical Engineering, 102(10), 3639-3660.

[31] Venkatadri, K., Bég, O. A., Bég, T. A., & Kuharat, S. (2024). Galerkin FEM simulation of natural convection in an annular porous medium-based solar collector system. International Journal of Ambient Energy, 45(1), 2358078.

[32] Venkatadri, K. (2022). Radiative magneto-thermogravitational flow in a porous square cavity with viscous heating and Hall current effects: A numerical study of ψ–v scheme. Heat Transfer, 51(7), 6705-6723.

[33] Hussain, M., Hanif, Z., Hussain, M. et al. Nonlinear radiative MHD flow of ternary nanofluid with Darcy–Forchheimer porous media: entropy generation analysis. J Therm Anal Calorim (2025). https://doi.org/10.1007/s10973-024-13785-2

[34] Abd-Elmonem, A., Ahmad, H., Garalleh, H. A., Atta, G., Amjad, M., Suoliman, N. A., ... & Hussain, S. M. (2025). Machine learning and differential transform simulation in analysing the ionic liquid (EtSO4) based ternary hybrid flow over a curved geometry. Journal of Molecular Liquids, 127109.

[35] Madubueze, C. E., Ajao, S., Akanni, J. O., Fatmawati, F., & Chazuka, Z. (2025). Impact of environmental contamination on Lassa fever transmission dynamics: a mathematical modelling approach. *Eur. Phys. J. Plus* 140, 202. https://doi.org/10.1140/epjp/s13360-025-06123-4.

[36] Akanni, J. O., Fatmawati, F., Ajao, S., Asamoah, J. K. K., & Abimbade, S. F. (2024), Mathematical model of COVID-19 dynamics in the presence of multiple controls. *Quality and Quantity* (2024). https://doi.org/10.1007/s11135-024-01975-x

[37] Abidemi, A., Akanni, J.O. Dynamics of illicit drug use and banditry population with optimal control strategies and cost-effectiveness analysis. *Comp. Appl. Math.* 41, 53 (2022). https://doi.org/10.1007/s40314-022-01760-2